

Vortex states in superconductors with strong Pauli-paramagnetic effect

Masanori Ichioka and Kazushige Machida

Department of Physics, Okayama University, Okayama 700-8530, Japan

(Dated: October 25, 2018)

Using the quasiclassical theory, we analyze the vortex structure of strong-paramagnetic superconductors. There, induced paramagnetic moments are accumulated exclusively around the vortex core. We quantitatively evaluate the significant paramagnetic effect in the H -dependence of various quantities, such as low temperature specific heat, Knight shift, magnetization and the flux line lattice (FLL) form factor. The anomalous H -dependence of the FLL form factor observed by the small angle neutron scattering in CeCoIn₅ is attributable to the large paramagnetic contribution.

PACS numbers: 74.25.Op, 74.25.Ha, 74.25.Jb, 74.70.Tx

I. INTRODUCTION

Recent two seemingly quite independent activities prompt us to cope those in a unified way because two typical experiments in each field suggest the vortex structure associated with strong influence of the *mismatched* Fermi surface, namely two Fermi levels for up and down spins are different; One is in the rotating fermion superfluids of neutral ⁶Li atom gases under the population imbalance.^{1,2,3,4} The other is heavy fermion superconductors with Zeeman-shifted Fermi surfaces under an applied field H . A heavy fermion compound CeCoIn₅ is a prime candidate of a superconductor with strong Pauli-paramagnetic effect, where at higher fields the upper critical field H_{c2} changes to the first order phase transition^{5,6,7} and new Fulde-Ferrell-Larkin-Ovchinnikov (FFLO) state appears.^{8,9,10,11,12,13,14,15} In the FFLO states, the pair potential is considered to have periodic spatial modulation in addition to the vortex modulation.^{16,17,18,19,20,21,22,23,24,25} It is because Cooper pairs of up- and down-spins acquire non-zero momentum for the center of mass coordinate of the Cooper pair by the Fermi surface splitting of up- and down-spin electron bands due to Zeeman shift. The Fermi surface splitting is also an origin of the Pauli-paramagnetic pair breaking and the appearance of paramagnetic moments. Therefore, even when the vortex states do not enter to the FFLO state yet, the strong paramagnetic effects may seriously contribute to the vortex state in superconductors.

It is expected that, in the presence of strong paramagnetic effect, observed quantized vortices in both systems of atomic gases and solid states should have universal common properties that are absent in conventional vortex picture. As for the rotating atomic gas under population imbalance within a trap potential, the vortex states were studied by Bogoliubov-de Gennes theory in the configuration of single vortex.⁴ There, paramagnetic moments are enhanced in the vortex core region, and the vortex core structure is related to the spectral evolution of quasiparticles around the vortex in the presence of Zeeman shift. Thus, also in solid states it is necessary to study the vortex states in superconductors with strong paramagnetic effect, clarifying the exotic vortex core structure of pair potential, paramagnetic moments,

internal magnetic field distributions, and local electronic states. These paramagnetic effects also give significant contributions to bulk properties, such as specific heat, paramagnetic susceptibility, or magnetizations.

In some heavy fermion superconductors, the paramagnetic effects due to Zeeman shift are important to understand the properties of the vortex states, because the superconductivity survives until under high magnetic fields due to the effective mass enhancement. The paramagnetic contributions are eminent at higher fields. For example, the H -dependence of low temperature specific heat $C(H)$ is often used to distinguish the presence of nodes in the pairing potential. The Sommerfeld coefficient $\gamma(H) = \lim_{T \rightarrow 0} C(H)/T \propto H$ in s -wave full gap superconductors, and $\gamma(H) \propto \sqrt{H}$ by the Volovik effect in d -wave pairing with line nodes.^{26,27,28,29} The curves of $\gamma(H)$ are expected to smoothly recover to the normal state value towards H_{c2} . However, in some heavy fermion superconductors, $C(H)$ deviates from these curves. In CeCoIn₅, $C(H)$ shows concave curves, i.e., $C(H) \propto H^\alpha$ ($\alpha > 1$) at higher fields.^{30,31,32} This behavior is difficult to be understood only by effects of the pairing symmetry. A similar $C(H)$ behavior is observed also in UBe₁₃.³³ The experimental data of magnetization curve $M_{\text{total}}(H)$ in CeCoIn₅ show a concave curve at higher fields, instead of a conventional convex curve.⁷ As an anomalous behavior of CeCoIn₅, the small angle neutron scattering (SANS) experiment reported the H -dependence of flux line lattice (FLL) form factor determined from the Bragg intensity.³⁴ While the form factor shows exponential decay as a function of H in many superconductors, it keeps almost constant at lower fields for $H \parallel c$ in CeCoIn₅. As for properties of CeCoIn₅, the contribution of antiferromagnetic fluctuation is also proposed in addition to the strong paramagnetic effect.^{15,35,36,37} Therefore, it is expected to study whether properties of vortex states in CeCoIn₅ are theoretically explained only by the paramagnetic effect. Theoretical studies of the H -dependences also help us to estimate strength of the paramagnetic effect from experimental data of the H -dependences in various superconductors.

In this paper, based on the selfconsistent microscopic calculation of quasiclassical Eilenberger theory,^{27,28,29,38,39,40} we study the spatial structure of the

vortex states in the presence of the paramagnetic effect by Zeeman-shift.^{25,41,42,43} We will clarify the paramagnetic effect on the vortex core structure, calculating the pair potential, paramagnetic moment, internal magnetic field, and local electronic states. We also study the paramagnetic effect by quantitatively estimating the H -dependence of low temperature specific heat, Knight shift, magnetization and FLL form factors, and show the relation of the H -dependence behaviors and the strength of paramagnetic effect. The anomalous field-dependence of FLL form factor observed by SANS experiment³⁴ is explained by the strong paramagnetic effect.

Previous works in the selfconsistent quasiclassical calculation were mainly applied to the vortex state in the absence of paramagnetic effects, and successfully estimate local electronic states around the vortex core and the H -dependence of the low temperature specific heat, studying the effect of the pairing symmetry,^{27,28,44} gap anisotropy,²⁹ and multi-band structure.⁴⁵ The selfconsistent calculation of the pair potential is necessary for quantitatively valid evaluation of the vortex states, since we have to use the correct vortex core size in the calculation at each field and temperature. As for previous quasiclassical studies on the strong paramagnetic effect on the vortex state, there were some works focusing on the FFLO vortex states.^{25,42} Without FFLO modulation but with strong paramagnetic effect, many studies were done along $H_{c2}(T)$, and there were few studies far from H_{c2} . The quasiclassical study on the H -dependence of the specific heat and magnetization were done by Adachi *et al.* at $T = 0.4T_c$, using Landau level expansion.⁴¹ In this paper, we study the H -dependence at $T = 0.1T_c$, solving the Eilenberger equation numerically by the explosion method^{39,40} in the vortex lattice state, and also study the vortex core structure including local electronic states, and the H -dependence of paramagnetic susceptibility and the FLL form factors.

After giving our formulation of quasiclassical theory in Sec. II, we study the paramagnetic effect on the H -dependence of paramagnetic susceptibility and low temperature specific heat in Sec. III. In Sec. IV, we show the paramagnetic contributions on the vortex core structure, and the local electronic state in the presence of Zeeman shift. In Sec. V, we estimate the H -dependence of FLL form factor, and discuss the anomalous H -dependence observed by SANS in CeCoIn₅. The paramagnetic effect on the magnetization curve is presented in Sec. VI, and the last section is devoted to summary and discussions.

II. QUASICLASSICAL THEORY INCLUDING PARAMAGNETIC CONTRIBUTION

We calculate the spatial structure of the vortex lattice state by quasiclassical Eilenberger theory in the clean limit,^{27,28,29,38,39,40} including the paramagnetic effects due to the Zeeman term $\mu_B B(\mathbf{r})$, where $B(\mathbf{r})$ is the flux density of the internal field and μ_B is a renor-

malized Bohr magneton.^{25,41,42,43} The quasiclassical theory is quantitatively valid when $\xi \gg 1/k_F$ (k_F is the Fermi wave number, and ξ is the superconducting coherence length), which is satisfied in most of superconductors in solid states. The quasiclassical Green's functions $g(\omega_n + i\mu B, \mathbf{k}, \mathbf{r})$, $f(\omega_n + i\mu B, \mathbf{k}, \mathbf{r})$, and $f^\dagger(\omega_n + i\mu B, \mathbf{k}, \mathbf{r})$ are calculated in the vortex lattice state by the Eilenberger equation

$$\begin{aligned} (\omega_n + i\mu B + \tilde{\mathbf{v}} \cdot (\nabla + i\mathbf{A})) f &= \Delta \phi g, \\ (\omega_n + i\mu B - \tilde{\mathbf{v}} \cdot (\nabla - i\mathbf{A})) f^\dagger &= \Delta^* \phi^* g, \end{aligned} \quad (1)$$

where $g = (1 - ff^\dagger)^{1/2}$, $\text{Reg} > 0$, $\tilde{\mathbf{v}} = \mathbf{v}/v_{F0}$, and $\mu = \mu_B B_0/\pi k_B T_c$. We mainly consider the d -wave pairing case for a pairing function, $\phi(\mathbf{k}) = \sqrt{2} \cos 2\theta$, as suggested in CeCoIn₅.^{5,31} \mathbf{k} is the relative momentum of the Cooper pair, and \mathbf{r} is the center-of-mass coordinate of the pair. We consider the case of two-dimensional cylindrical Fermi surface, $\mathbf{k} = k_F(\cos \theta, \sin \theta)$, where $0 \leq \theta < 2\pi$. The Fermi velocity is given by $\mathbf{v} = v_{F0}(\cos \theta, \sin \theta)$. Throughout this paper, length, temperature, and magnetic field are scaled by R_0 , T_c , and B_0 , respectively. Here, $R_0 = \hbar v_{F0}/2\pi k_B T_c$, $B_0 = \hbar c/2|e|R_0^2$. Matsubara frequency $\omega_n = (2n+1)\pi T$, energy E , and pair potential Δ are scaled by $\pi k_B T_c$. Since magnetic fields are applied to the z axis direction, in the symmetric gauge the vector potential $\mathbf{A}(\mathbf{r}) = \frac{1}{2}\bar{\mathbf{B}} \times \mathbf{r} + \mathbf{a}(\mathbf{r})$, where $\bar{\mathbf{B}} = (0, 0, \bar{B})$ is a uniform flux density and $\mathbf{a}(\mathbf{r})$ is related to the internal field $\mathbf{B}(\mathbf{r}) = \bar{\mathbf{B}} + \nabla \times \mathbf{a}(\mathbf{r})$. The unit cell of the vortex lattice is given by $\mathbf{r} = s_1(\mathbf{u}_1 - \mathbf{u}_2) + s_2\mathbf{u}_2$ with $-0.5 \leq s_i \leq 0.5$ ($i=1, 2$), $\mathbf{u}_1 = (a, 0, 0)$ and $\mathbf{u}_2 = (a/2, a_y, 0)$. In the d -wave pairing, we consider the case of square vortex lattice, i.e., $a_y/a = 1/2$, where the nearest neighbor vortices are located to the nodal direction. In the d -wave superconductors, this square lattice configuration is stable at higher fields.^{27,34}

The pair potential is selfconsistently calculated by

$$\Delta(\mathbf{r}) = g_0 N_0 T \sum_{0 < \omega_n \leq \omega_{\text{cut}}} \left\langle \phi^*(\mathbf{k}) (f + f^{\dagger*}) \right\rangle_{\mathbf{k}} \quad (2)$$

with $(g_0 N_0)^{-1} = \ln T + 2T \sum_{0 < \omega_n \leq \omega_{\text{cut}}} \omega_n^{-1}$. $\langle \dots \rangle_{\mathbf{k}}$ indicates the Fermi surface average. We use $\omega_{\text{cut}} = 20k_B T_c$. The vector potential for the internal magnetic field is selfconsistently determined by

$$\nabla \times (\nabla \times \mathbf{A}) = \nabla \times \mathbf{M}_{\text{para}}(\mathbf{r}) - \frac{2T}{\tilde{\kappa}^2} \sum_{0 < \omega_n} \langle \mathbf{v}_F \text{Im} g \rangle_{\mathbf{k}}, \quad (3)$$

where we consider both the diamagnetic contribution of supercurrent in the last term and the contribution of the paramagnetic moment $\mathbf{M}_{\text{para}}(\mathbf{r}) = (0, 0, M_{\text{para}}(\mathbf{r}))$ with

$$M_{\text{para}}(\mathbf{r}) = M_0 \left(\frac{B(\mathbf{r})}{B} - \frac{2T}{\mu_B \bar{B}} \sum_{0 < \omega_n} \langle \text{Im} \{g\} \rangle_{\mathbf{k}} \right). \quad (4)$$

The normal state paramagnetic moment $M_0 = (\mu/\tilde{\kappa})^2 \bar{B}$, $\tilde{\kappa} = B_0/\pi k_B T_c \sqrt{8\pi N_0}$ and N_0 is the density of states

(DOS) at the Fermi energy in the normal state. We solve Eq. (1) and Eqs. (2)-(4) alternately, and obtain selfconsistent solutions as in previous works,^{27,40,45} under a given unit cell of the vortex lattice. The unit cell is divided to 41×41 mesh-points, where we obtain the quasiclassical Green's functions, $\Delta(\mathbf{r})$, $M_{\text{para}}(\mathbf{r})$ and $\mathbf{A}(\mathbf{r})$. When we solve Eq. (1) by the explosion method, we estimate $\Delta(\mathbf{r})$ and $\mathbf{A}(\mathbf{r})$ at arbitrary positions by the interpolation from their values at the mesh points, and by the periodic boundary condition of the unit cell including the phase factor due to the magnetic field.^{27,39,40,45}

Using Doria-Gubernatis-Rainer scaling,^{43,46} we obtain the relation of \bar{B} and the external field H as

$$H = \left(1 - \frac{\mu^2}{\tilde{\kappa}^2}\right) \left(\bar{B} + \left\langle (B(\mathbf{r}) - \bar{B})^2 \right\rangle_{\mathbf{r}} / \bar{B}\right) + \frac{T}{\tilde{\kappa}^2 \bar{B}} \left\langle \sum_{0 < \omega_n} \langle \mu B(\mathbf{r}) \text{Im} \{g\} + \frac{1}{2} \text{Re} \left\{ \frac{(f^\dagger \Delta + f \Delta^*)g}{g+1} \right\} \right\rangle_{\mathbf{r}} + \omega_l \text{Re} \{g - 1\} \Big|_{\mathbf{k}}, \quad (5)$$

where $\langle \dots \rangle_{\mathbf{r}}$ indicates the spatial average. We consider the case of large Ginzburg-Landau (GL) parameter $\kappa_{\text{GL}} \sim \tilde{\kappa} = 89$ and low temperature $T/T_c = 0.1$. For the two-dimensional Fermi surface, $\tilde{\kappa} = (7\zeta(3)/8)^{1/2} \kappa_{\text{GL}} \sim \kappa_{\text{GL}}$.⁴⁷ In these parameters, $|\bar{B} - H| < 10^{-4} B_0$.

When we calculate the electronic states, we solve Eq. (1) with $i\omega_n \rightarrow E + i\eta$. The local density of states (LDOS) is given by $N(\mathbf{r}, E) = N_\uparrow(\mathbf{r}, E) + N_\downarrow(\mathbf{r}, E)$, where

$$N_\sigma(\mathbf{r}, E) = N_0 \langle \text{Re} \{g(\omega_n + i\sigma\mu B, \mathbf{k}, \mathbf{r})\} \Big|_{i\omega_n \rightarrow E + i\eta} \rangle_{\mathbf{k}} \quad (6)$$

with $\sigma = 1$ (-1) for up (down) spin component. We typically use $\eta = 0.01$. The DOS is obtained by the spatial average of the LDOS as $N(E) = N_\uparrow(E) + N_\downarrow(E) = \langle N(\mathbf{r}, E) \rangle_{\mathbf{r}}$.

III. FIELD DEPENDENCE OF PARAMAGNETIC SUSCEPTIBILITY AND ZERO-ENERGY DOS

First, we discuss the field dependence of zero-energy DOS $\gamma(H) = N(E=0)/N_0$ and paramagnetic susceptibility $\chi(H) = \langle M_{\text{para}}(\mathbf{r}) \rangle_{\mathbf{r}}/M_0$, which are normalized by the normal state values. From low temperature specific heats C , we obtain $\gamma(H) \propto C/T$ experimentally. And $\chi(H)$ is observed by the Knight shift in NMR experiments, which measure the paramagnetic component induced by an external field via the hyperfine coupling between a nuclear spin and conduction electrons. In d -wave pairing, $\chi(H)$ shows \sqrt{H} -behavior at low fields.⁴⁸

As shown in Fig. 1, γ (dashed lines) and χ (solid lines) show almost the same behavior at low temperatures. First, we see the case of d -wave pairing with line nodes in Fig. 1(a). There $\gamma(H)$ and $\chi(H)$ describe \sqrt{H} -like recovery smoothly to the normal state value ($\gamma = \chi = 1$ at H_{c2}) in the case of negligible paramagnetic effect ($\mu = 0.02$).^{26,27,28,29} With increasing the

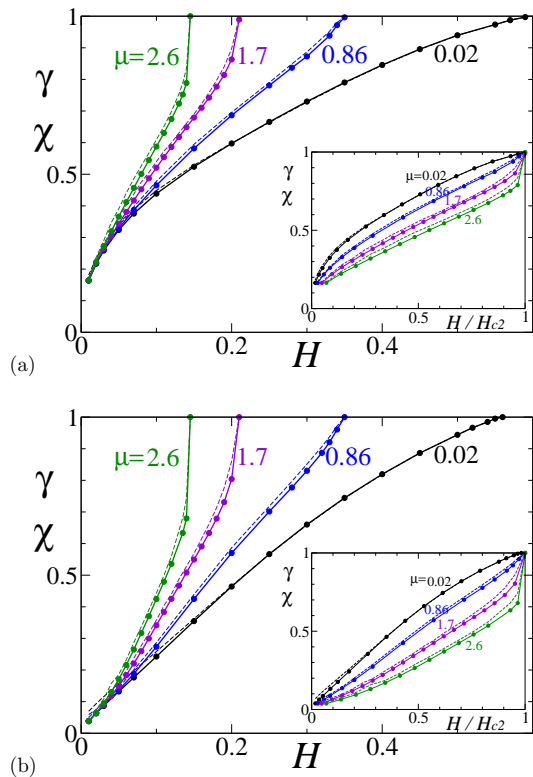


FIG. 1: (color online) The magnetic field dependence of the paramagnetic susceptibility $\chi(H)$ (solid lines) and the zero-energy DOS $\gamma(H)$ (dashed lines) at $T = 0.1T_c$ for various paramagnetic parameters $\mu = 0.02, 0.86, 1.7$, and 2.6 in the d -wave (a) and s -wave (b) pairing cases. The insets show same data as a function of H/H_{c2} .

paramagnetic parameter μ , H_{c2} is suppressed and the Volovik curve $\gamma(H) \propto \sqrt{H}$ gradually changes into curves with a concave curvature. For large μ , H_{c2} changes to first order phase transition.⁴¹ We note that at lower fields all curves exhibit a \sqrt{H} behavior because the paramagnetic effect ($\propto H$) is not effective. Further increasing H , $\gamma(H)$ behaves quite differently. There we find a turning point field which separates a convex curve at lower H and a concave curve at higher H . This inflection point increases as μ decreases. In the inset of Fig. 1, we plot $\gamma(H)$ and $\chi(H)$ as a function of H/H_{c2} . The overall H -dependence at $0 < H < H_{c2}$ can be used to analyze experimental data, in order to estimate the strength of the paramagnetic effect, μ .

To examine effects of the pairing symmetry, we show $\gamma(H)$ and $\chi(H)$ also for s -wave pairing $\phi(\mathbf{k}) = 1$ in Fig. 1(b), where we use the triangular lattice configuration $a_y/a = \sqrt{3}/2$. In the H -dependence of $\gamma(H)$ and $\chi(H)$, differences by the vortex lattice configuration of triangular or square are small. The difference in the H -dependences of Figs. 1(a) and 1(b) at low fields comes from the gap structure of the pairing function. In the full gap case of s -wave pairing, $\gamma(H)$ and $\chi(H)$ show H -linear-like behavior at low fields. With increasing the

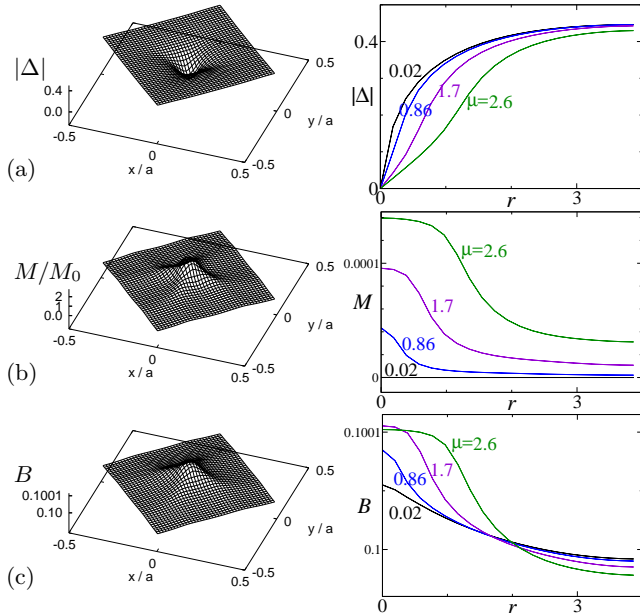


FIG. 2: (color online) Spatial structure of the pair potential (a), paramagnetic moment (b) and internal magnetic field (c) at $T = 0.1T_c$ and $\bar{B} = 0.1B_0$, where $a = 11.2R_0$, in d -wave pairing. The left panels show $|\Delta(\mathbf{r})|$, $M_{\text{para}}(\mathbf{r})$, and $B(\mathbf{r})$ within a unit cell of the square vortex lattice at $\mu = 1.7$. The right panels show the profiles along the trajectory r from the vortex center to the midpoints between nearest neighbor vortices. $\mu = 0.02, 0.86, 1.7$, and 2.6 .

paramagnetic effect, H -linear behaviors gradually change into curves with a concave curvature. As seen in Figs. 1(a) and 1(b), paramagnetic effects appear similarly at high fields both for s -wave and d -wave pairings.

The concave curves of the specific heat at higher fields by strong paramagnetic effect were also presented in Ref. 41 at $T = 0.4T_c$. In the present calculation, the concave curves are confirmed even at low temperature $T = 0.1T_c$, where $C/T \sim \gamma(H)$ without large specific heat jump at H_{c2} . In $\gamma(H)$ at low T , the differences of s -wave and d -wave pairings at lower fields are clearly seen.

IV. PARAMAGNETIC CONTRIBUTION ON VORTEX CORE STRUCTURE

In order to understand the contribution of the paramagnetic effect on the vortex structure, we illustrate the local structures of the pair potential $|\Delta(\mathbf{r})|$, paramagnetic moment $M_{\text{para}}(\mathbf{r})$, and internal magnetic field $B(\mathbf{r})$ within a unit cell of the vortex lattice in Fig. 2. Since we assume d -wave pairing with the line node gap here, the vortex core structure is deformed to fourfold symmetric shape around a vortex core.^{27,49} It is noted that the paramagnetic moment is enhanced exclusively around the vortex core, as shown in Fig. 2(b) where the four ridges

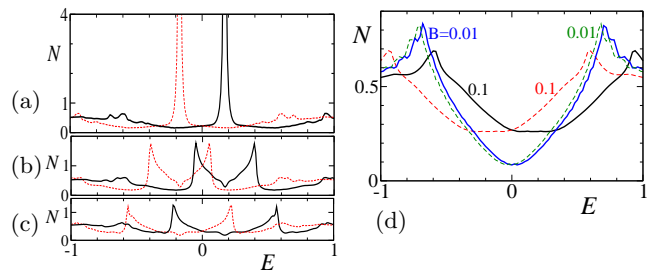


FIG. 3: (color online) Local density of states at $r/R_0 = 0$ (a), 0.8 (b) and 1.6 (c) from the vortex center towards the nearest neighbor vortex direction in d -wave pairing. Solid lines show $N_{\uparrow}(\mathbf{r}, E)/N_0$ for up-spin electrons, and dashed lines show $N_{\downarrow}(\mathbf{r}, E)/N_0$ at $\bar{B} = 0.1B_0$. $\mu = 1.7$ and $T = 0.1T_c$. (d) Spatially-averaged DOS at $\bar{B}/B_0 = 0.1$ and 0.01 in d -wave pairing. Solid lines show $N_{\uparrow}(E)/N_0$ for up-spin electrons, and dashed lines show $N_{\downarrow}(E)/N_0$.

of paramagnetic moment are extended towards the anti-nodal directions from the core. Since the contribution of the paramagnetic vortex core is enhanced with increasing μ , internal field $B(\mathbf{r})$ consisting of diamagnetic and paramagnetic contributions is further enhanced around the vortex core by the paramagnetic effect, as shown in Fig. 2(c). When μ is large, the pair potential $|\Delta(\mathbf{r})|$ is slightly suppressed around the paramagnetic vortex core, and the vortex core radius is enlarged, as shown in Fig. 2(a).

The enhancement of $M_{\text{para}}(\mathbf{r})$ around vortex core is related to spatial structure of the LDOS $N_{\sigma}(\mathbf{r}, E)$. As shown in Fig. 3(a), the LDOS spectrum shows *zero-energy peak* at the vortex center, but the spectrum is shifted to $E = \pm\mu\bar{B}$ due to Zeeman shift. The peak states at $E > 0$ is empty for $N_{\uparrow}(E, \mathbf{r})$, and the peak at $E < 0$ is occupied for $N_{\downarrow}(E, \mathbf{r})$. Therefore, from the relation

$$M_{\text{para}}(\mathbf{r}) = -\mu_B \int_{-\infty}^0 (N_{\uparrow}(E, \mathbf{r}) - N_{\downarrow}(E, \mathbf{r})) dE, \quad (7)$$

large $M_{\text{para}}(\mathbf{r})$ appears due to the local imbalance of up- and down-spin occupation around the vortex core. As shown in Figs. 3(b) and 3(c), increasing the distance from the vortex center, the peak of the spectrum is split into two peaks, which are shifted to higher and lower energies, respectively. When one of split peaks crosses $E = 0$, the imbalance of up- and down-spin occupation is decreased. Thus, $M_{\text{para}}(\mathbf{r})$ is suppressed outside of vortex cores.

In Fig. 3(d), we present the spectrum of spatially-averaged DOS. In the DOS spectrum, peaks of the LDOS are smeared by the spatial average. Because of the flat spectrum at low energies, paramagnetic susceptibility $\chi(H)$ shows almost the same H -behavior as the zero-energy DOS $\gamma(H) \sim N(E = 0)$ even for large μ , as shown in Fig. 1, while $\chi(H)$ counts the DOS contribution in the energy range $|E| < \mu H$, i.e., $\chi(H) \sim \int_0^{\mu H} N_{\uparrow}(E) dE / \mu H$ from Eq. (7).

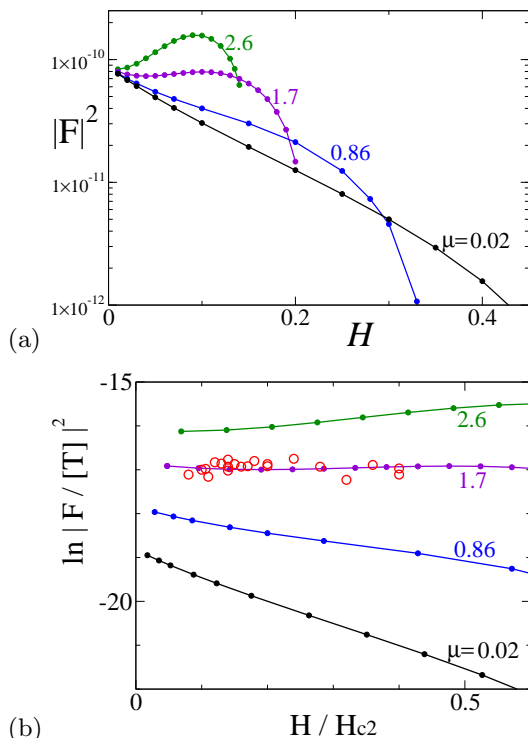


FIG. 4: (color online) Field dependence of FLL form factor $F_{1,0}$ for $\mu = 0.02, 0.86, 1.7,$ and 2.6 at $T = 0.1T_c$ in d -wave pairing. (a) $|F_{1,0}|^2$ is plotted as a function of H . The vertical axis is in logarithmic scale. (b) We plot $\ln |F_{1,0}|^2$ as a function of H/H_{c2} , where $F_{1,0}$ is scaled so that H_{c2} for each μ corresponds to 5 [T]. Open circles are experimental data in CeCoIn₅ observed by SANS experiment.³⁴

V. FIELD DEPENDENCE OF FLUX LINE LATTICE FORM FACTOR

One of the best ways to directly see the accumulation of the paramagnetic moment around the vortex core is to observe the Bragg scattering intensity of the FLL via SANS experiment. The intensity of the (h, k) -diffraction peak is given by $I_{h,k} = |F_{h,k}|^2 / |\mathbf{q}_{h,k}|$ with the wave vector $\mathbf{q}_{h,k} = h\mathbf{q}_1 + k\mathbf{q}_2$, $\mathbf{q}_1 = (2\pi/a, -\pi/a_y, 0)$ and $\mathbf{q}_2 = (2\pi/a, \pi/a_y, 0)$. The Fourier component $F_{h,k}$ is given by $B(\mathbf{r}) = \sum_{h,k} F_{h,k} \exp(i\mathbf{q}_{h,k} \cdot \mathbf{r})$. The intensity of the main peak at $(h, k) = (1, 0)$ in the SANS for FLL observation probes the magnetic field contrast between the vortex cores and the surrounding.

We calculate the field dependence of $|F_{1,0}|^2$, which is shown in Fig. 4. In the case of negligible paramagnetic effect ($\mu = 0.02$), $|F_{1,0}|^2$ decreases exponentially as a function of H . This is a result for the d -wave pairing at low T in the clean limit. With increasing paramagnetic effect, the decreasing slope of $|F_{1,0}|^2$ becomes gradual, and changes to increasing functions of H at lower fields in extremely strong paramagnetic case ($\mu = 2.6$). This is because $|F_{1,0}|$ includes enhanced paramagnetic contribution proportional to μH , reflecting the enhanced internal

field around the vortex core, shown in Fig. 2(c), by the paramagnetic moment.

The SANS experiment in CeCoIn₅ reported that $|F_{1,0}|^2$ is almost constant as a function of H within the field range $0.08 \leq H/H_{c2} \leq 0.4$ ($0.4[\text{T}] \leq H \leq 2.0[\text{T}]$) for $H \parallel c$.³⁴ This behavior is reproduced by our calculation for $\mu \sim 1.7$. There, $|F_{1,0}|^2$ shows flat behavior at low fields, since the paramagnetic contribution increasing with H compensates the conventional decrease of $|F_{1,0}|^2$ as a function of H . For the comparison to the experimental data, we plot $\ln |F_{1,0}|^2$ as a function of H/H_{c2} at lower fields in Fig. 4(b). There, unit of the magnetic field in the calculated data for each μ is rescaled so that H_{c2} corresponds to 5 [T], i.e., H_{c2} in CeCoIn₅ for $H \parallel c$. For quantitative accordance of the results for $\mu = 1.7$ with the experimental data, we tune the GL parameter as $\tilde{\kappa} = 89$. The variations of internal fields are roughly proportional to $\tilde{\kappa}^{-2}$, as seen from Eq. (3). Changing $\tilde{\kappa}$, we can shift curves in Fig. 4(b) towards the vertical direction. The slopes of the curves in Fig. 4(b) are determined by the paramagnetic effect. With increasing μ , the negative slope becomes gradual, and even changes to positive slope. When the paramagnetic effect is negligible ($\mu = 0.02$), $\ln |F_{1,0}|^2$ decreases by 2 in the field range $0.1 < H/H_{c2} < 0.5$, which corresponds to the exponential decay as a function of H , as expected in conventional superconductors (also see the theoretical curves in Ref. 34). For the large paramagnetic case $\mu = 1.7$, $\ln |F_{1,0}|^2$ does not decrease as a function of H , which accords with the experimental data [circles in Fig. 4(b)] of SANS experiments. The anomalous H -dependence of the SANS intensity in CeCoIn₅ can be explained by the strong paramagnetic effect, and suggests $\mu \sim 1.7$. When $\mu \sim 1.7$, H_{c2} is about 38% suppressed by the paramagnetic pair breaking from the value of no paramagnetic effect, as seen in Fig. 1. The strong paramagnetic contributions are also considered as an origin of new FFLO phase and first order H_{c2} phase transition at higher fields.

The purpose of this discussion was to demonstrate that the paramagnetic effect can change the slope of $\ln |F_{1,0}|^2$ as a function of H , and that in the case of strong paramagnetic effect $|F_{1,0}|^2$ does not show exponential decay. We note that for further nice fitting to the experimental data, there is a room to include the effect by the Fermi surface anisotropy or by deformations of the vortex lattice configuration.

VI. FIELD DEPENDENCE OF MAGNETIZATION

We discuss the paramagnetic effect on the magnetization curves. In Fig. 5(a), magnetization curves are presented as a function of H for various T at $\mu = 1.7$. The magnetization $M_{\text{total}} = \bar{B} - H$ includes both the diamagnetic and the paramagnetic contributions. It is seen that $M_{\text{total}}(H)$ exhibits a sharp rise near H_{c2} by the paramagnetic pair breaking effect, and that $M_{\text{total}}(H)$

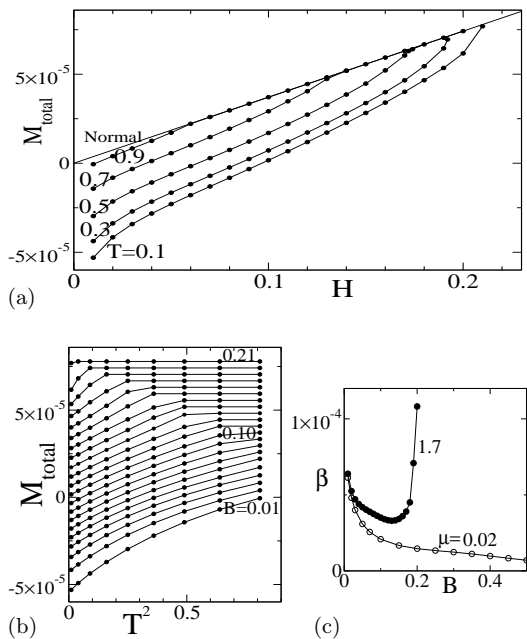


FIG. 5: (color online) (a) Magnetic field dependence of magnetization M_{total} for $\mu = 1.7$ at $T/T_c = 0.1, 0.3, 0.5, 0.7, 0.9$ and 1.0 (normal state) in d -wave pairing. (b) M_{total} as a function of T^2 at $\bar{B} = 0.01, 0.02, 0.03, \dots, 0.21$. (c) H -dependence of factor $\beta(H)$ at $\mu = 0.02$ and 1.7.

has concave curvature at higher fields, instead of a conventional convex curvature. These behaviors are seen in experimental data of CeCoIn₅,⁷ and previous calculation at $T = 0.4T_c$.⁴¹

In Fig. 5(b), M_{total} is plotted as a function of T^2 for various \bar{B} . We fit these curves as $M_{\text{total}}(T, H) = M_0 + \frac{1}{2}\beta(H)T^2 + O(T^3)$ at low T . The slope $\beta(H) = \lim_{T \rightarrow 0} \partial^2 M_{\text{total}} / \partial T^2$ decreases on raising H at lower fields. However, at higher fields approaching H_{c2} , the slope $\beta(H)$ sharply increases. Thus, as shown in Fig. 5(c), $\beta(H)$ as a function of H exhibits a minimum at intermediate H and rapid increase near H_{c2} by the paramagnetic effect when $\mu = 1.7$. This is contrasted with the case of negligible paramagnetic effect ($\mu = 0.02$), where $\beta(H)$ is a decreasing function of H until H_{c2} .

The behavior of $\beta(H)$ is consistent with that of $\gamma(H)$, since there is a relation $\beta(H) \propto \partial \gamma(H) / \partial H$ obtained from a thermodynamic Maxwell's relation $\partial^2 M_{\text{total}} / \partial T^2 = \partial(C/T) / \partial B$ and $B \sim H$.⁴¹ In Fig. 1, we see that for $\mu = 1.7$ the slope of $\gamma(H)$ is decreasing function of H at low H , but changes to increasing function near H_{c2} . This behavior correctly reflects the H -dependence of $\beta(H)$. The rapid increase near H_{c2} is clearly seen at lower temperatures, compared with the results at higher temperatures.⁴¹

VII. SUMMARY AND DISCUSSIONS

We studied the vortex states in the presence of strong paramagnetic effect by selfconsistent quasiclassical calculations, which can be used for quantitative estimate of the vortex states even far from H_{c2} . Calculating the spatial structure of the vortex states and local electronic states, we clarified the paramagnetic effects on the vortex core structure. There, the core radius is enlarged and the internal field around the core is further enhanced, due to the enhanced paramagnetic moments at the vortex core.

Qualitatively estimating the H -dependence of low temperature specific heat, Knight shift, magnetization, and FLL form factor, we showed the relationship between the H -dependence behaviors and the strength of the paramagnetic effect. The specific heat, Knight shift, and magnetization show rapid increase near H_{c2} , due to the paramagnetic pair breaking which is eminent at higher fields. The anomalous H -dependences of FLL form factor of SANS experiment³⁴ in CeCoIn₅ are also explained by the strong paramagnetic effect. This reflects the paramagnetic vortex core structure, affecting the internal field distribution. These theoretical studies of the H -dependences help us to evaluate the strength of the paramagnetic effect from the experimental data of the H -dependences in various superconductors. For example, analyses for Sr₂RuO₄, TmNi₂B₂C and URu₂Si₂ are given elsewhere.^{50,51,52}

As for CeCoIn₅, our analysis of FLL form factor in SANS experiment suggests $\mu \sim 1.7$. This indicates strong paramagnetic effect, so that H_{c2} is about 38% suppressed by the paramagnetic pair breaking from the value of no paramagnetic effect. On the other hand, when we compare the H -dependence of the specific heat with the experimental data,³² experimental data $\gamma(H) \sim C/T$ also show the concave curve at higher fields, as suggested in our calculation. However, at lower fields, $\gamma(H)$ is much smaller than that expected by our theoretical calculation. This discrepancy indicates that experimental data may include other additional contributions, such as antiferromagnetic fluctuations, or H -dependent bulk properties other than the conduction electrons. Therefore, in order to understand the H -dependences of the vortex state properties in CeCoIn₅, we need further careful studies by the collaboration of experimental and theoretical studies.

Acknowledgments

The authors are grateful for useful discussions and communications with T. Mizushima, H. Adachi, N. Nakai, K. Kumagai, and M.R. Eskildsen.

¹ M.W. Zwierlein, A. Schirotzek, C.H. Schunck, and W. Ketterle, Science **311**, 492 (2006).

² G.B. Partridge, W. Li, R.I. Kamar, Y. Liao, and R.G.

- Hulet, *Science* **311**, 503 (2006).
- ³ K. Machida, T. Mizushima, and M. Ichioka, *Phys. Rev. Lett.* **97**, 120407 (2006), and references cited therein.
 - ⁴ M. Takahashi, T. Mizushima, M. Ichioka, and K. Machida, *Phys. Rev. Lett.* **97**, 180407 (2006).
 - ⁵ K. Izawa, H. Yamaguchi, Y. Matsuda, H. Shishido, R. Settai, and Y. Onuki, *Phys. Rev. Lett.* **87**, 057002 (2001).
 - ⁶ A. Bianchi, R. Movshovich, N. Oeschler, P. Gegenwart, F. Steglich, J.D. Thompson, P.G. Pagliuso, and J.L. Sarrao, *Phys. Rev. Lett.* **89**, 137002 (2002).
 - ⁷ T. Tayama, A. Harita, T. Sakakibara, Y. Haga, H. Shishido, R. Settai, and Y. Onuki, *Phys. Rev. B* **65**, 180504(R) (2002).
 - ⁸ A. Bianchi, R. Movshovich, C. Capan, P.G. Pagliuso, and J.L. Sarrao, *Phys. Rev. Lett.* **91**, 187004 (2003).
 - ⁹ H. A. Radovan, N.A. Fortune, T.P. Murphy, S.T. Hannahs, E.C. Palm, S.W. Tozer, and D. Hall, *Nature (London)* **425**, 51 (2003).
 - ¹⁰ T. Watanabe, Y. Kasahara, K. Izawa, T. Sakakibara, Y. Matsuda, C. J. van der Beek, T. Hanaguri, H. Shishido, R. Settai, and Y. Onuki, *Phys. Rev. B* **70**, 020506(R) (2004).
 - ¹¹ C. Capan, A. Bianchi, R. Movshovich, A.D. Christianson, A. Malinowski, M.F. Hundley, A. Lacerda, P.G. Pagliuso, and J.L. Sarrao, *Phys. Rev. B* **70**, 134513 (2004).
 - ¹² C. Martin, C.C. Agosta, S.W. Tozer, H.A. Radovan, E.C. Palm, T.P. Murphy, and J.L. Sarrao, *Phys. Rev. B* **71**, 020503(R) (2005).
 - ¹³ K. Kakuyanagi, M. Saitoh, K. Kumagai, S. Takashima, M. Nohara, H. Takagi, and Y. Matsuda, *Phys. Rev. Lett.* **94**, 047602 (2005).
 - ¹⁴ K. Kumagai, M. Saitoh, T. Oyaizu, Y. Furukawa, S. Takashima, M. Nohara, H. Takagi, and Y. Matsuda, *Phys. Rev. Lett.* **97**, 227002 (2006).
 - ¹⁵ Y. Matsuda and H. Shimahara, *J. Phys. Soc. Jpn.* **76**, 051005 (2007).
 - ¹⁶ P. Fulde and R.A. Ferrell, *Phys. Rev.* **135**, A550 (1964).
 - ¹⁷ A.I. Larkin and Y.N. Ovchinnikov, *Sov. Phys. JETP* **20**, 762 (1965).
 - ¹⁸ K. Machida and H. Nakanishi, *Phys. Rev. B* **30**, 122 (1984).
 - ¹⁹ Y. Tanaka, Y. Asano, M. Ichioka, and S. Kashiwaya, *Phys. Rev. Lett.* **98**, 077001 (2007).
 - ²⁰ M. Tachiki, S. Takahashi, P. Gegenwart, M. Weiden, M. Lang, C. Geibel, F. Steglich, R. Modler, C. Paulsen, and Y. Onuki, *Z. Physik B* **100**, 369 (1996).
 - ²¹ M. Houzet and A. Buzdin, *Phys. Rev. B* **63**, 184521 (2001).
 - ²² H. Adachi and R. Ikeda, *Phys. Rev. B* **68**, 184510 (2003).
 - ²³ R. Ikeda and H. Adachi, *Phys. Rev. B* **69**, 212506 (2004).
 - ²⁴ T. Mizushima, K. Machida, and M. Ichioka, *Phys. Rev. Lett.* **95**, 117003 (2005); *ibid.* **94**, 060404 (2005).
 - ²⁵ M. Ichioka, H. Adachi, T. Mizushima, and K. Machida, *Phys. Rev. B* **76**, 014503 (2007).
 - ²⁶ G.E. Volovik, *JETP Lett.* **58**, 469 (1993).
 - ²⁷ M. Ichioka, A. Hasegawa, and K. Machida, *Phys. Rev. B* **59**, 184 (1999); *ibid.* **59**, 8902 (1999).
 - ²⁸ P. Miranović, N. Nakai, M. Ichioka, and K. Machida, *Phys. Rev. B* **68**, 052501 (2003).
 - ²⁹ N. Nakai, P. Miranović, M. Ichioka, and K. Machida, *Phys. Rev. B* **70**, 100503(R) (2004).
 - ³⁰ S. Ikeda, H. Shishido, M. Nakashima, R. Settai, D. Aoki, Y. Haga, H. Harima, Y. Aoki, T. Namiki, H. Sato, and Y. Onuki, *J. Phys. Soc. Jpn.* **70**, 2248 (2001).
 - ³¹ H. Aoki, T. Sakakibara, H. Shishido, R. Settai, Y. Onuki, P. Miranović, and K. Machida, *J. Phys.: Condens. Matter* **16**, L13 (2004).
 - ³² K. Deguchi, S. Yonezawa, S. Nakatsuji, Z. Fisk, and Y. Maeno, *J. Magn. Magn. Mater.* **310**, 587 (2007).
 - ³³ A. P. Ramirez, C. M. Varma, Z. Fisk, and J. L. Smith, *Philos. Mag. B* **79** (1999) 111.
 - ³⁴ L. DeBeer-Schmitt, C.D. Dewhurst, B.W. Hoogenboom, C. Petrovic, and M.R. Eskildsen, *Phys. Rev. Lett.* **97**, 127001 (2006).
 - ³⁵ A. Bianchi, R. Movshovich, I. Vekhter, P.G. Pagliuso, and J.L. Sarrao, *Phys. Rev. Lett.* **91**, 257001 (2003).
 - ³⁶ J. Paglione, M.A. Tanatar, D.G. Hawthorn, E. Boaknin, R.W. Hill, F. Ronning, M. Sutherland, L. Taillefer, C. Petrovic, and P.C. Canfield, *Phys. Rev. Lett.* **91**, 246405 (2003).
 - ³⁷ B.-L. Young, R.R. Urbano, N.J. Curro, J.D. Thompson, J.L. Sarrao, A.B. Vorontsov, and M.J. Graf, *Phys. Rev. Lett.* **98**, 036402 (2007).
 - ³⁸ G. Eilenberger, *Z. Phys.* **214**, 195 (1968).
 - ³⁹ U. Klein, *J. Low Temp. Phys.* **69**, 1 (1987).
 - ⁴⁰ M. Ichioka, N. Hayashi, and K. Machida, *Phys. Rev. B* **55**, 6565 (1997).
 - ⁴¹ H. Adachi, M. Ichioka, and K. Machida, *J. Phys. Soc. Jpn.* **74**, 2181 (2005).
 - ⁴² U. Klein, D. Rainer, and H. Shimahara, *J. Low Temp. Phys.* **118**, 91 (2000).
 - ⁴³ K. Watanabe, T. Kita, and M. Arai, *Phys. Rev. B* **71**, 144515 (2005).
 - ⁴⁴ M. Ichioka and K. Machida, *Phys. Rev. B* **65**, 224517 (2002).
 - ⁴⁵ M. Ichioka, K. Machida, N. Nakai, and P. Miranović, *Phys. Rev. B* **70**, 144508 (2004).
 - ⁴⁶ M.M. Doria, J.E. Gubernatis, and D. Rainer, *Phys. Rev. B* **41**, 6335 (1990).
 - ⁴⁷ P. Miranović and K. Machida, *Phys. Rev. B* **67**, 092506 (2003).
 - ⁴⁸ G.-q. Zheng, H. Ozaki, Y. Kitaoka, P. Kuhns, A.P. Reyes, and W.G. Moulton, *Phys. Rev. Lett.* **88**, 077003 (2002).
 - ⁴⁹ M. Ichioka, N. Hayashi, N. Enomoto, and K. Machida, *Phys. Rev. B* **53**, 15316 (1996).
 - ⁵⁰ K. Machida and M. Ichioka, arXiv:0706.1426.
 - ⁵¹ L. DeBeer-Schmitt, M.R. Eskildsen, M. Ichioka, K. Machida, N. Jenkins, C.D. Dewhurst, A.B. Abrahamsen, S.L. Bud'ko, and P.C. Canfield, unpublished.
 - ⁵² K. Yano, T. Sakakibara, T. Tayama, M. Yokoyama, H. Amitsuka, Y. Homma, P. Miranović, M. Ichioka, Y. Tsutsumi, and K. Machida, unpublished.